Extended Abstract, 42nd AIAA Aero. Sci. Mtg., Reno NV, Jan 6, 2004

Implementation of Premixed Equilibrium Chemistry Capability in OVERFLOW

M. E. Olsen *NASA Ames Research Center
Moffett Field, CA 94035
Y. Liu †NASA Ames Research Center
Moffett Field, CA 94035
M. Vinokur ‡Eloret Corp.
Sunnyvale , CA 94087
T. Olsen §ELORET Corp.
Sunnyvale , CA 94087

An implementation of premixed equilibrium chemistry has been completed for the OVERFLOW code, a chimera capable, complex geometry flow code widely used to predict transonic flowfields. The implementation builds on the computational efficiency and geometric generality of the solver.

Nomenclature

$\tilde{\gamma}$	$\rho c^2/p$
ϵ	internal energy($\int_0^T c_v dT$)
ϵ_T	$\epsilon + \frac{1}{2}(u^2+v^2+w^2)$
η	self similar wedge wall distance $((z-z_w)/x)$
κ	turbulent kinetic energy: $\frac{1}{2}\sum u_i' u_i'$
μ_T	turbulent eddy viscosity
ρ	mass per unit volume
θ	angle along sphere surface(degrees)
ξ	dimensionless wedge axial distance (x/L)
c	isentropic sound speed
h_T	stagnation enthalpy ($\epsilon+p/\rho+\frac{1}{2}(u^2+v^2+w^2)$)
L	wedge length
p	static pressure
s	entropy
S_{ij}	$\frac{1}{2}\left(\frac{\partial u_i}{\partial x_j}+\frac{\partial u_j}{\partial x_i}\right)$
T	static temperature
u, v, w	cartesian velocity components
x, y, z	cartesian position coordinates

Introduction

Building on the successful application of the perfect gas version of OVERFLOW to hypersonic flowfields,[1] the next step in implementing finite rate chemistry capability in OVERFLOW is the generalization of the gas model from single species perfect gas to allow pressure and temperature as arbitrary functions of density and internal energy. The specific thermodynamic model used was that of Liu and Vinokur.[2] This model provides pressure and temperature for an equilibrium mixture of air over a wide temperature and pressure range.

Method

The Reynolds averaged Navier-Stokes equations, written in conservation law form are

$$\frac{\partial Q}{\partial t}+\frac{\partial F}{\partial x}+\frac{\partial G}{\partial y}+\frac{\partial H}{\partial z} = 0 \qquad (1)$$

Where

$$Q = [\rho, \rho u, \rho v, \rho w, \rho\epsilon] \qquad (2)$$

$$F = \left[\rho u, \rho u^2+p+\tau_{xx}, \rho uv+\tau_{xy}, \rho uw+\tau_{xz}\right.$$
$$\left.\rho u(\epsilon_T+p+\tau_{xx})+v\tau_{xy}+w\tau_{xz}+k\frac{\partial T}{\partial x}\right] \qquad (3)$$

$$G = \left[\rho v, \rho vu+\tau_{yx}, \rho v^2+p+\tau_{yy}, \rho vw+\tau_{yz},\right.$$
$$\left.\rho v(\epsilon_T+p+\tau_{yy})+w\tau_{yz}+u\tau_{yx}+k\frac{\partial T}{\partial y}\right] \qquad (4)$$

$$H = \left[\rho u, \rho wu+\tau_{zx}, \rho wv+\tau_{zy}, \rho w^2+p+\tau_{zz},\right.$$
$$\left.\rho w(\epsilon_T+p+\tau_{zz})+u\tau_{zx}+v\tau_{zy}+k\frac{\partial T}{\partial z}\right] \qquad (5)$$

where, we assume a simple Boussinesq type stress-strain relationship for the turbulence,

$$\tau_{ij} = 2(\mu+\mu_T)S_{ij}-\frac{2}{3}\rho\kappa\delta_{ij} \qquad (6)$$

The thermodynamic relation for pressure $p = p(\rho, \epsilon)$ is used in place of the perfect gas assumption($p = \rho(\gamma-1)\epsilon$) in computing the fluxes of the momentum and energy equations, and the thermodynamic relation

*Research Scientist, NASA Ames Research Center, Associate Fellow AIAA
†Research Scientist, NASA Ames Research Center
‡Senior Research Scientist, Eloret, Associate Fellow AIAA
§Research Scientist, ELORET, Member AIAA

for temperature $T = T(\rho, \epsilon)$ enters into these equations indirectly, in the evaluation of molecular viscosity and thermal conductivity.

Implicit solution requires the calculation of Euler Jacobians ($\frac{\partial F_\epsilon}{\partial Q}$, $\frac{\partial G_\epsilon}{\partial Q}$, and $\frac{\partial H_\epsilon}{\partial Q}$) and for diagonalized methods, their eigenvectors and eigenvalues. The Euler fluxes are simply the Navier-Stokes fluxes with μ, μ_T, and k, set to zero. This generally involves an evaluation of the isentropic sound speed, c. The sound speed is derived from the partial derivatives of the pressure returned by the thermodynamics module, and it current implementation allows a capability more general than mixtures of perfect gases in chemical equilibrium.

This solver is actually capable of predicting flows of any simple compressible substance where pressure and temperature are functions of only density and internal energy. The sound speed is given by the general relation for isentropic sound speed $c^2 = \left.\frac{\partial p}{\partial \rho}\right|_s$ As we have a table lookup routine which returns values of p, T, $\left.\frac{\partial p}{\partial \rho}\right|_\epsilon$ $\left.\frac{\partial p}{\partial \epsilon}\right|_\rho$ $\left.\frac{\partial T}{\partial \rho}\right|_\epsilon$ $\left.\frac{\partial T}{\partial \epsilon}\right|_\rho$, we need to be able to get the sound speed in terms of these variables and their derivatives.

From the Gibbs equation for a simple compressible substance,

$$\begin{aligned} ds &= \frac{1}{T}(d\epsilon + p dv) \\ &= \frac{1}{T}(d\epsilon - p d\rho/\rho^2) \end{aligned} \tag{7}$$

we get the relations

$$\begin{aligned} \left.\frac{\partial \epsilon}{\partial \rho}\right|_s &= -p/\rho^2 \\ \left.\frac{\partial \epsilon}{\partial s}\right|_\rho &= 1/T \end{aligned} \tag{8}$$

which, along with the trivial relations

$$\begin{aligned} \left.\frac{\partial \rho}{\partial \rho}\right|_s &= 1 \\ \left.\frac{\partial \rho}{\partial s}\right|_\rho &= 0 \end{aligned} \tag{9}$$

allows us to transform the partial derivatives we have naturally as a result of the bicubic spline: $\left.\frac{\partial p}{\partial \rho}\right|_\epsilon$, $\left.\frac{\partial p}{\partial \epsilon}\right|_\rho$ into derivatives where $[\rho, s]$ are the independent variables. Thus we may calculate the sound speed from

$$\begin{aligned} c^2 &= \left.\frac{\partial p}{\partial \rho}\right|_s \\ &= \left.\frac{\partial p}{\partial \rho}\right|_\epsilon + \left.\frac{\partial p}{\partial \epsilon}\right|_\rho \left.\frac{\partial \epsilon}{\partial \rho}\right|_s \end{aligned} \tag{10}$$

This is the relation used to give the sound speed, which is implemented by calculating an effective γ,

$$\begin{aligned} \bar{\gamma} &= \rho c^2/p \\ &= \frac{\rho}{p}\left.\frac{\partial p}{\partial \rho}\right|_\epsilon + \frac{1}{\rho}\left.\frac{\partial p}{\partial \epsilon}\right|_\rho \end{aligned} \tag{11}$$

Implementation

The base code used is OVERFLOW[3] which is a finite difference, chimera capable, complex geometry flow code widely used for perfect gas prediction. Matrix dissipation is used with central space differencing and multigrid to provide a rapid, robust solution method suitable for high speed flow with strong shock waves.[1]

OVERFLOW was modified to replace the perfect gas model built into the code with an arbitrary gas model, where the pressure and sound speeds are functions of the density and internal energy, as given in Liu.[2,4] An efficient table lookup method returns the pressure and temperature and their derivatives corresponding to a given value of $[\rho, \epsilon]$. A bicubic spline is used to produce smooth interpolations of both functions and their derivatives.

Four additional variables are added to the conservative variables $[\rho, \rho u, \rho v, \rho w, \rho\epsilon]$. The four additional field variables are $[p/p_\infty, T/T_\infty, Pr, p/(\rho R_\infty T)]$. These variables are obtained from the conservative variables at the start of each iteration, before the laminar viscosity is calculated. The perfect gas assumptions are then replaced by the use of the calculated pressures(in the momentum and energy fluxes, and their derivatives), temperatures (in the viscosity and conductivity calculations), and sound speed (in the implicit jacobian calculations).

2nd order central flux differencing combined with matrix dissipation[5,6] is used in forming the right hand side residuals, similar to the scheme used for perfect gas solutions.[1] The implicit solution method used is the Pulliam–Chaussee diagonal algorithm, with the eigensystem[7] the same as used to implement the matrix dissipation. Roe averaging is used in forming the matrices in the dissipation scheme.

The multigrid method[6] has been modified to enhance the robustness of the method. The original multigrid method used a linear interpolation of the conservative variables to map the coarse grid solution onto the next finer grid. This interpolation was replaced with a linear interpolation of the variables $[\rho, u, v, w, \epsilon]$, which ensures a positive value of ϵ on the finer grid if ϵ is positive on the coarser grid.

Results

Inviscid Wedge Flow

This flowfield is a self similar flowfield useful for gauging the ability to capture shocks at oblique angles to the grid, and to obtain the external inviscid

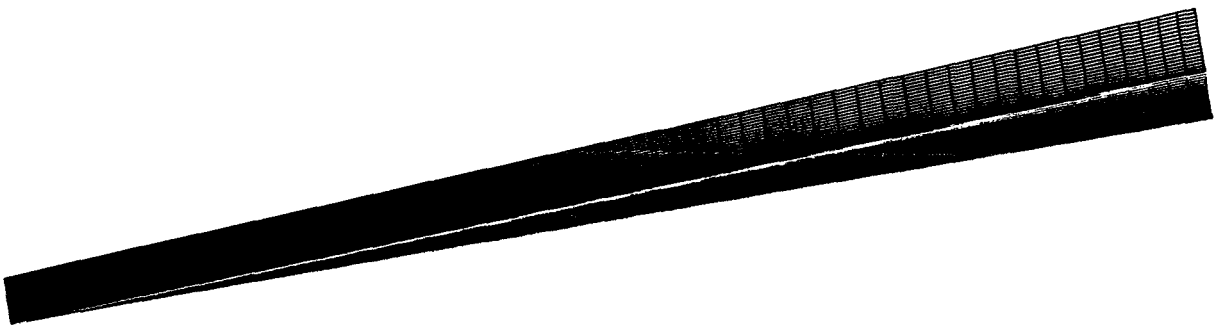

Fig. 1 10°M=25 Inviscid Wedge Grid, Colored by Axial Velocity

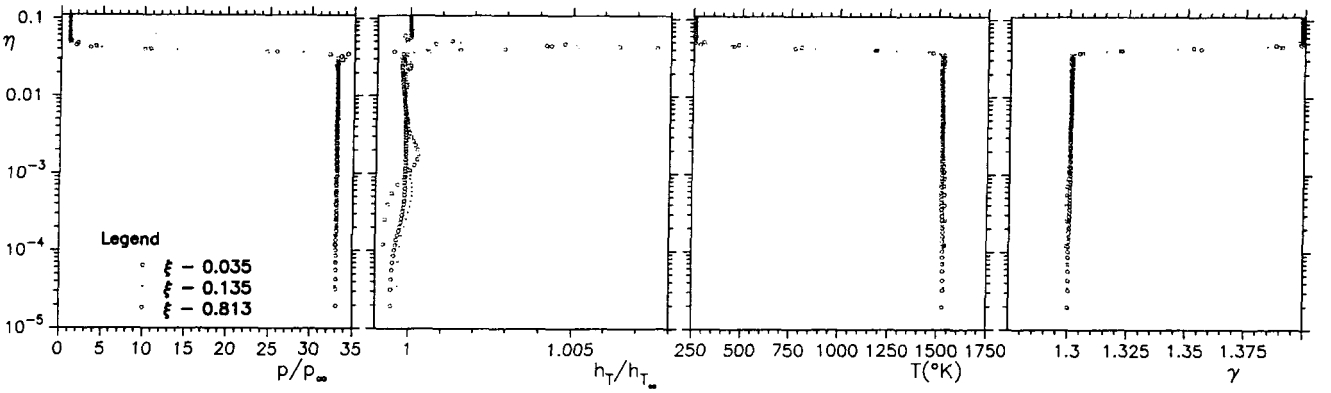

Fig. 2 Inviscid M=25 Wedge, Profiles of Pressure, Total Enthalpy, Temperature and γ

flowfield downstream of the shock. The case considered here is a 10° wedge, at M=25.083, with freestream static conditions of $p_\infty = 20.24$Pa, $T_\infty = 257$°K.

A converged solution is shown in Figure 1. The capture of the oblique shock is clearly demonstrated, with uniform conditions obtained on both sides of the shock. The shock crosses the grid system obliquely, with the shock moving out one grid line for every two gridlines moved downstream.

Profiles of pressure, total enthalpy, temperature, and pressure are shown in Figure 2. The pressure profile shows minimal overshoot, with good similarity between the various axial locations The total enthalpy is well conserved (for this flowfield it is constant), with errors, even at the shock, less than 0.5%. Total enthalpy errors behind the shock are less than 0.1%. The post shock temperature reached in this flowfield is 1500°K, for which there is appreciable dissociation, as shown by the gamma variation from 1.4(freestream) to 1.3(post shock).

Inviscid Blunt Body Flow

This case is the inviscid flow past a blunt cylinder (Fig 3) over a range of freestream static pressure and Mach number. The pressure conditions range from p = 1Pa(h=80km) to p = 10KPa(h=16km). The

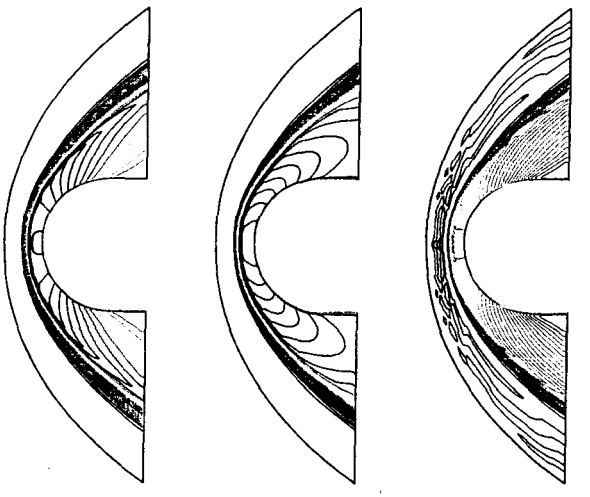

a) Pressure **b)** Temperature **c)** Density

Fig. 3 $M_\infty = 32$, p = 10Pa = Blunt Body Flowfield

Mach numbers range from $M_\infty = 8$(2.4km/sec) to $M_\infty = 32$(9.5km/sec). The solutions were obtained on a 101 × 129 grid suitable for computation of a perfect gas, so much of the grid lies outside the shock.

These solutions demonstrate the ability of the matrix dissipation to capture the shock over the wide

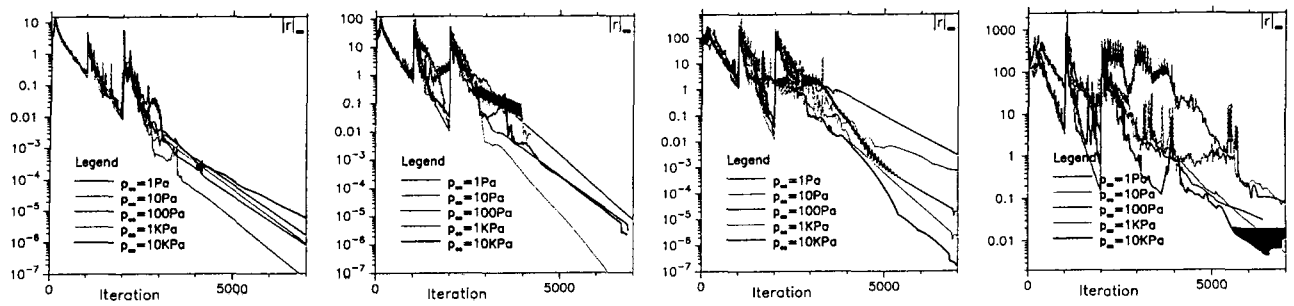

a) $M_\infty = 8$ b) $M_\infty = 16$ c) $M_\infty = 24$ d) $M_\infty = 32$

Fig. 4 Inviscid Cylinder Blunt Body Residual Histories

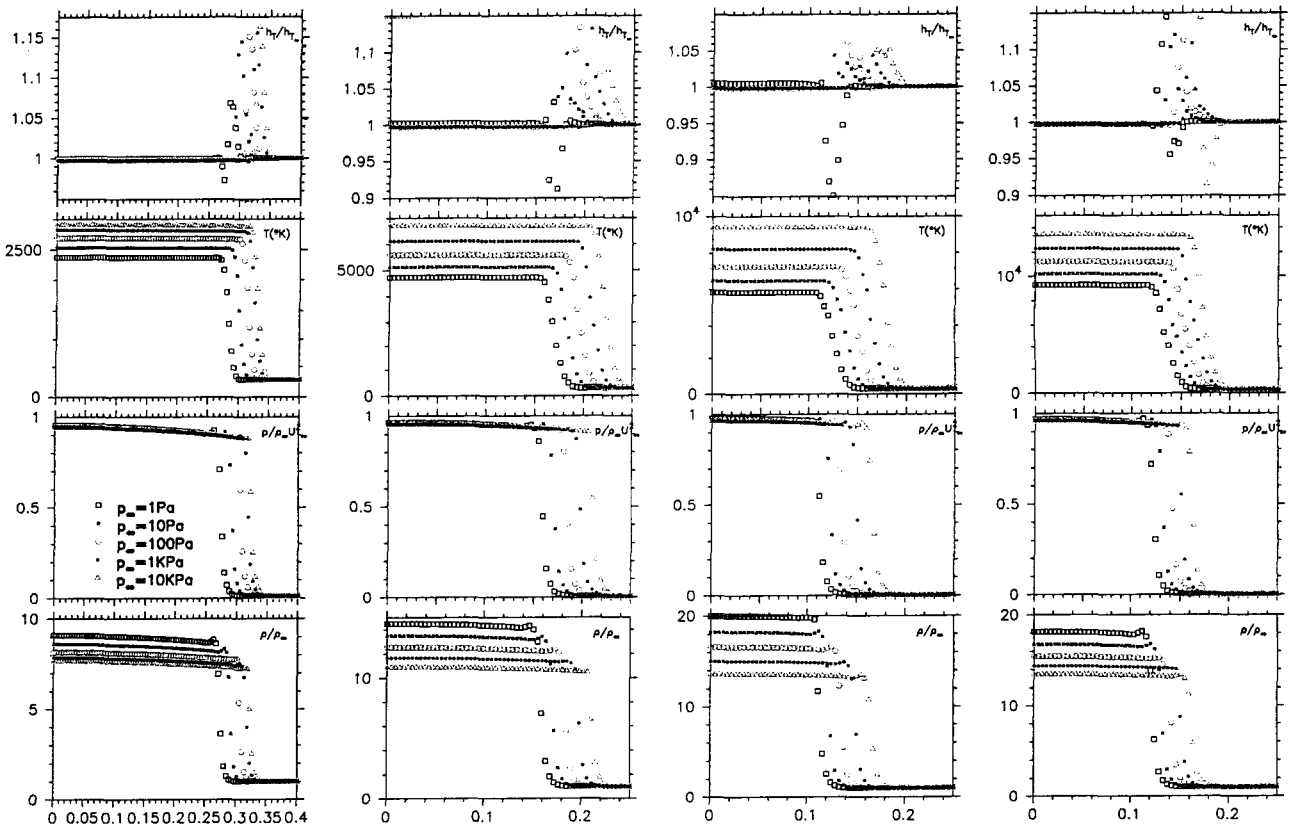

a) $M_\infty = 8$ b) $M_\infty = 16$ c) $M_\infty = 24$ d) $M_\infty = 32$

Fig. 5 Inviscid Cylinder Blunt Body Stagnation Line State

range of conditions representative of earth atmospheric reentry. The smoothing parameters are unchanged over this entire range of conditions, and only the M = 32 cases required an adjustment of the CFL(halved from the other conditions) to obtain convergence (Fig 4).

While all the cases show a similarity in the stagnation pressure profiles, (Fig 5) the variations of the temperature and density are more pronounced as the Mach number increases. At a fixed Mach number, a lower freestream pressure implies a lower post-shock temperature, as the dissociation is more complete at lower pressure. An interesting trend is evident in the density profiles. As the Mach number increase from 8 to 24, the post shock density increases, but from Mach 24 to Mach 32, there is a *decrease* in the post shock density especially at the higher pressures.

The preservation of total enthalpy across the shock is good at all Mach numbers. Along with being a check on the fidelity of the solution, this will be important in obtaining good heat transfer predictions in viscous flowfields. The pressure profiles in all cases are collapsed nicely when normalized by the Newtonian pressure, ρu_∞^2.

Viscous Flat Plate

As important as inviscid shock capturing capabilities are the abilities to predict heat transfer and skin

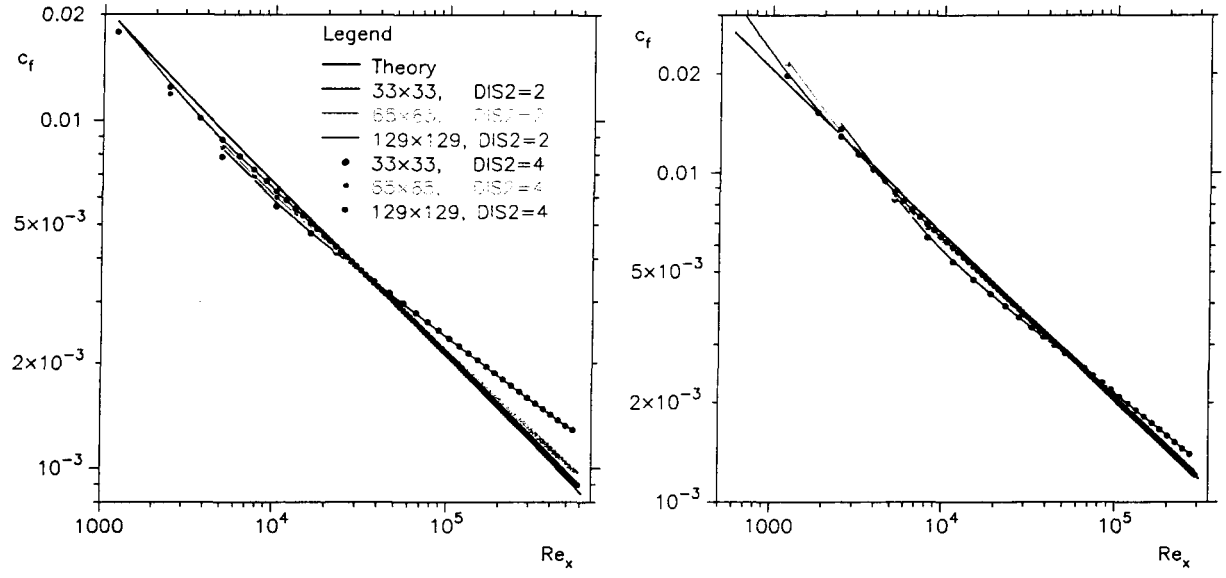

a) $M_\infty = 2$ b) $M_\infty = 4$

Fig. 6 Flat Plate Skin Friction Predictions

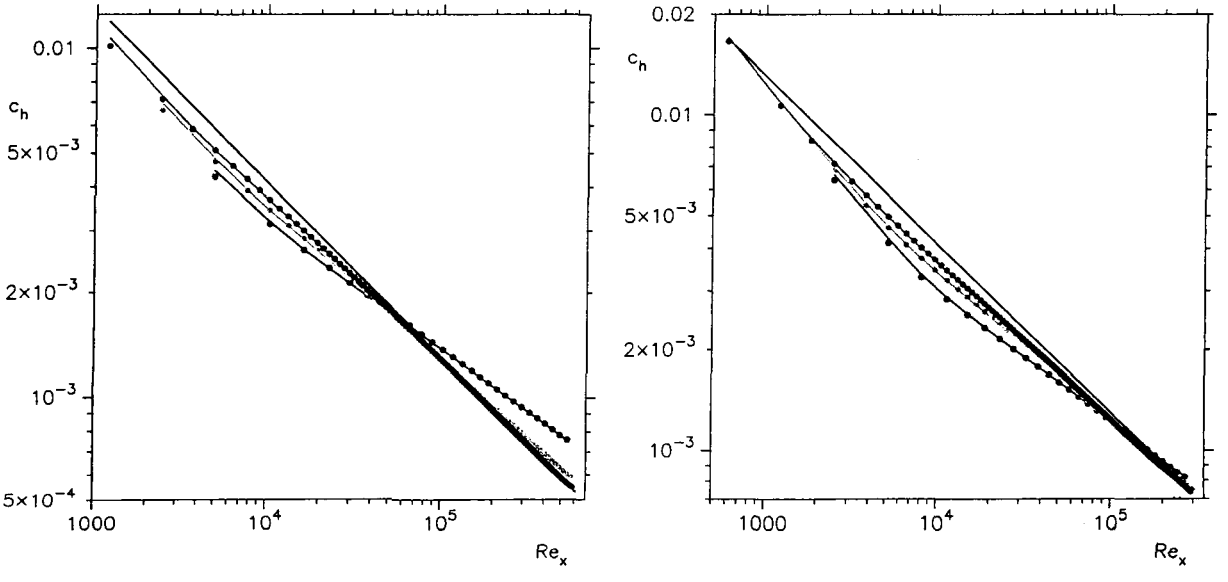

a) $M_\infty = 2$ b) $M_\infty = 4$

Fig. 7 Flat Plate Heat Transfer Predictions

friction. Solutions for a laminar flat plat at freestream Mach numbers of 2 and 4 were obtained on 3 grids, 129×129, 65×65, and 33×33. The skin friction predictions are all nicely in agreement with theory (Figure 6) and the heat transfer predictions (Figure 7) are similarly good. These predictions were obtained with the same dissipation parameters used to produce the inviscid wedge and cylinder solutions. Also shown are the skin friction predictions with the lowered dissipation settings, which agree quite well with the 'standard' dissipation settings.

Viscous Sphere

This case considers a viscous flow over a 1m radius sphere at $M_\infty = 17.6$, $p = 57.4$Pa, $T_\infty = 360°$K, as shown in figure 8. This case is the benchmark case for LAURA, (http://hefss.larc.nasa.gov). The viscous wall boundary condition was no slip, $T_w = 900°$K. The finest grid used was 65(streamwise) by 129 (wall normal), with a constant wall grid spacing of 0.5μm. Two coarser grids were derived by this one by choosing every other point (33×65), and every fourth point(17×33).

The stagnation streamlines for this case (Figure 9) are given in both external flow (linear in axial distance)

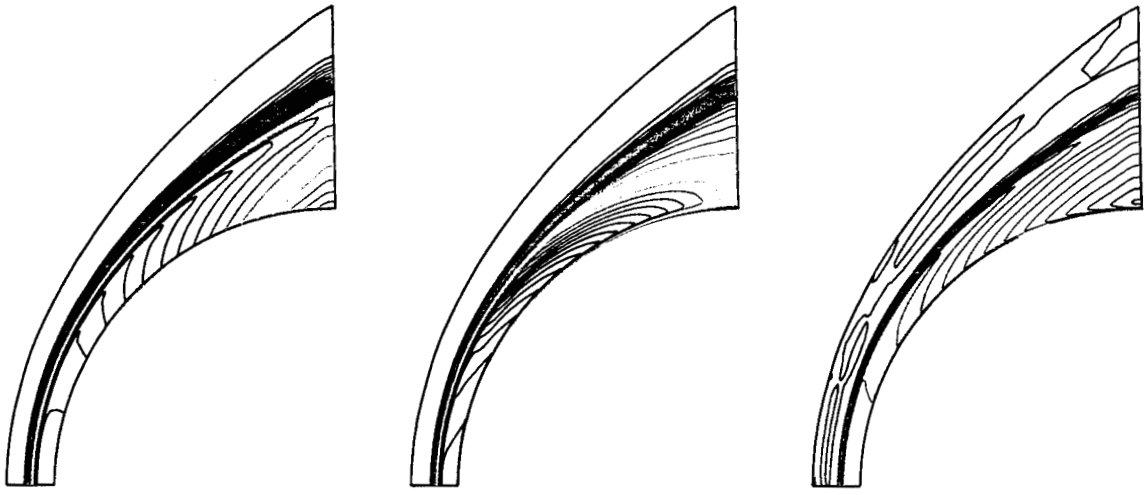

a) Pressure b) Temperature c) Density

Fig. 8 Viscous $M_\infty = 17.6$, p = 57.4Pa 1m Sphere

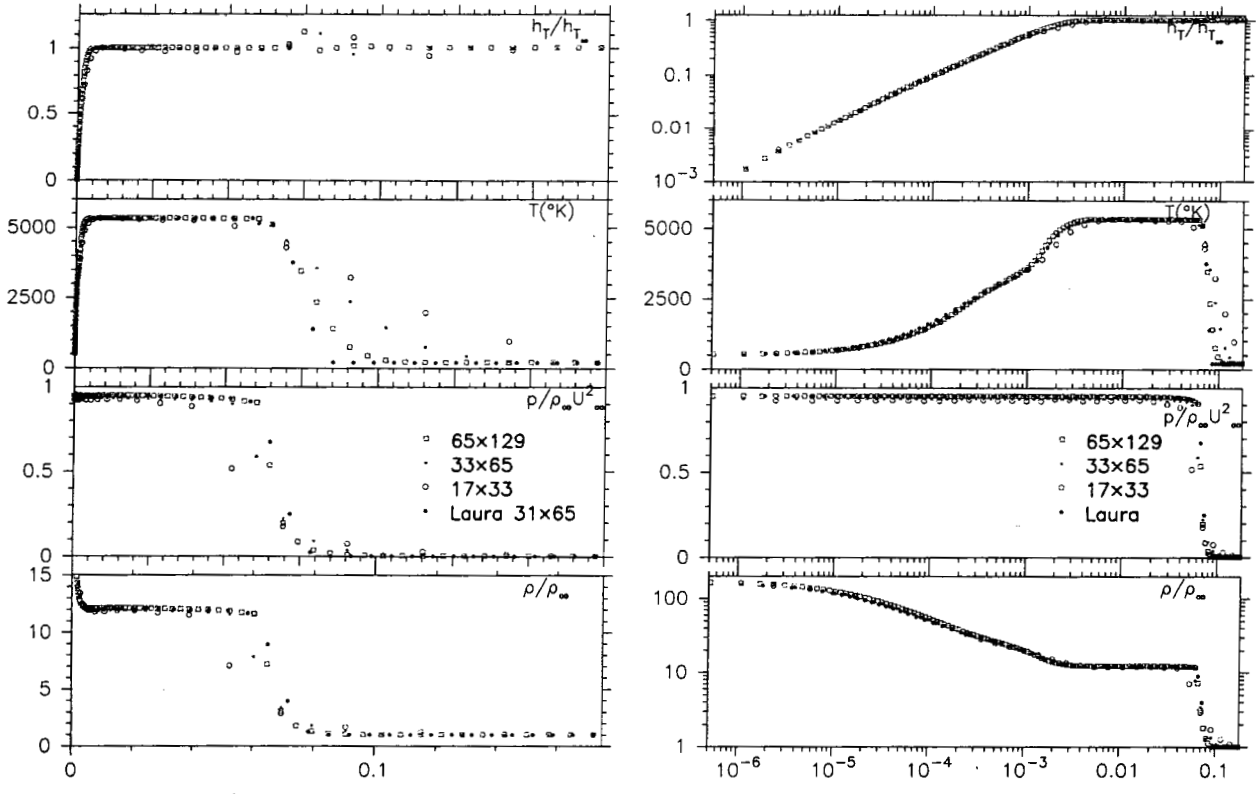

a) External Flow b) Boundary Layer

Fig. 9 Stagnation Profiles, $M_\infty = 17.6$, p = 57.4Pa 1m Sphere

and boundary layer(logarithmic in axial distance) coordinates. The pressure profile looks very similiar to the inviscid case (Figure 5), and agrees well with the prediction of LAURA, but here the stagnation enthalpy and static temperature variations are dominated by that of the boundary layer variations. The temperature predictions show the same boundary layer "lumpiness" predicted by LAURA, whereas the total enthalpy prediction is quite smooth over the same region. Heat transfer predictions(Figure 10) are similiar to those of the LAURA code.

High Enthalpy Nozzle Expansion

This case highlights the ability to predict flowfields with extreme expansion. T10-97 is one of the First Europe–U.S. High Speed Flow Database test cases.[8] This case documents to flowfield in the ONERA F4

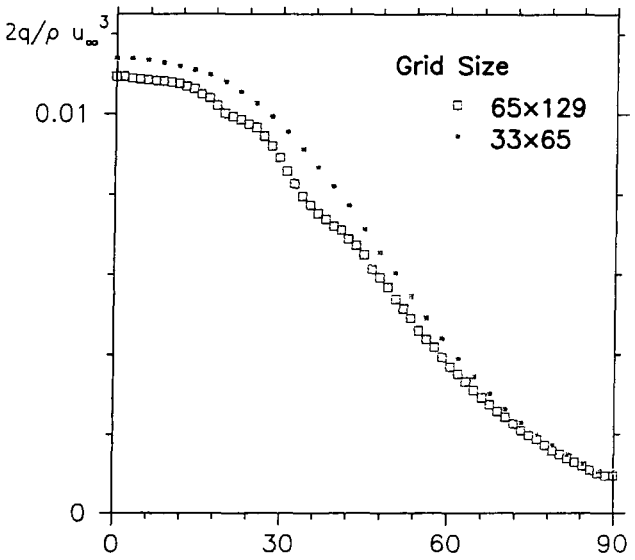

Fig. 10 Wall Heating Distribution, $M_\infty = 17.6$, p = 57.4Pa 1m Sphere

a) Density, Overall Flowfield

b) Reservoir Detail

Fig. 11 T10-97 (ONERA F4) Wind Tunnel Nozzle Flowfield

high enthalpy facility. The resevoir conditions are p = 373bar, $h_0 = 140T_\infty$, and the exhaust conditions are $T_\infty = 273°K$, $p_\infty = 68Pa$. The resevoir is charged with synthetic air, composed of $\frac{2}{9}O_2$ and $\frac{7}{9}N_2$ by mass fractions.

A sequence of three grids was again utilized, with the finest grid 513(Streamwise) × 129(WallNormal), and the coarser grids again created via 'bicimation'. The solutions for this case depend critically on the air thermodynanmic models,[8] and the current results (Figure 12) are consistent with the results of other equilibrium air codes utilized to simulate this case.

Conclusions

The present method shows promise for rapid prediction of complex flowfields where fully mixed chemical equilibrium is an appropriate approximation, and is another step in the overall goal of adding chemically reacting flow capability to OVERFLOW.

References

[1]Olsen, Michael E. and Dinesh K. Prabhu. "Application of OVERFLOW to Hypersonic Perfect Gas Flowfields". AIAA Paper 2001-2664, 2001.

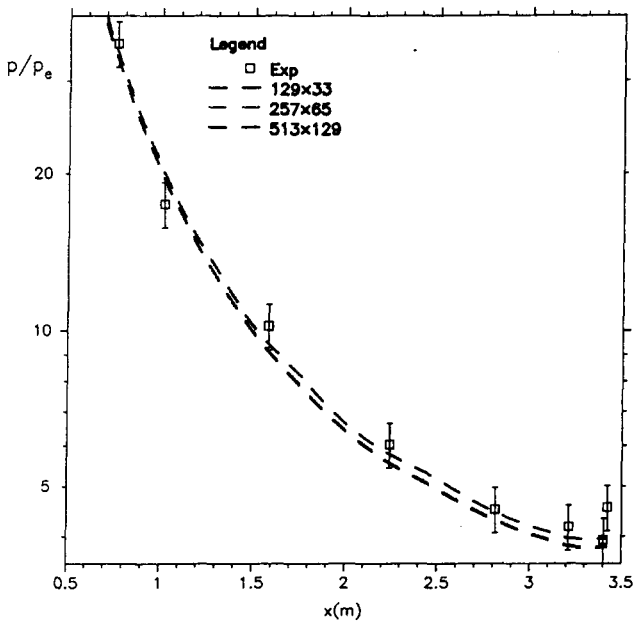

Fig. 12 Wall Pressure Distribution, T10-917 Test Case: Comparison with Experiment

[2]Liu, Yen and Vinokur, Marcel. "Equilibrium Gas Flow Computations. I. Accurate and Efficient Calculation of Equilibrium Gas Properties". AIAA Paper 89-1736, 1989.

[3]Buning, Pieter G. et al. Overflow user's manual. Version 1.8, NASA Ames Research Center, February 1998.

[4]Liu, Y. and M. Vinokur. "Equilibrium Gas Flow Computations. II. An analysis of Numerical Formulations of Conservation Laws". AIAA Paper 88-0127, Jan. 1988.

[5]Swanson, R. C. and Eli Turkel. "On Central–Difference and Upwind Schemes". *Journal of Computational Physics*, 101:292–306, 1992.

[6]Jespersen, D, Pulliam, T. H., and P.G. Buning. Recent enhancements to overflow. AIAA Paper 97-0664, January 1997.

[7]Liu, Yen and Marcel Vinokur. "Nonequilibrium Flow Computations. I. An Analysis of Numerical Formulations of Conservation Laws". *Journal of Computational Physics*, 83, No 2:373–396, August 1989.

[8]Sagnier, P. and Muylaert, M. "Synthesis of the Contributions to the Test Case T10-97 Wind Tunnel Nozzle". First Europe-US High Speed Flow Database Workshop-Part 2, November 12–14 2000, Naples, Italy, 1997.